INDEPENDENT URA MONITOR FOR GPS IIIC

Ronald Braff, Brian Bian and Curtis A. Shively

Center for Advanced Aviation System Development

The MITRE Corporation, McLean VA

ABSTRACT

To assure the integrity of critical navigation operations, the user range accuracy (URA) is envisioned to provide future users the means to rigorously bound the fault-free and fault-induced errors in the signal-in-space (SIS) from each GPS IIIC space vehicle (SV). This paper examines an independent URA monitor (IUM) that could be incorporated into the next generation GPS Control Segment (OCX) to assure that the broadcast URA bounds any errors in the broadcast SV ephemeris and clock correction parameters. The IUM operates on single or multiple snapshot data in order to maintain an independent and timely integrity assured URA for each OCX upload to an SV. It thus generates larger URAs than would be obtained when they are generated from continuous tracking data and an orbital model. A performance assessment, based on an example GPS IIIC constellation and covariance analysis, is used to estimate worldwide minimum monitorable URA values (MMUs) generated by the IUM.

To examine operational feasibility of the IUM, an analysis is presented for an application of GPS IIIC with IUM to the stringent integrity requirements of the Localizer Performance with Vertical guidance (LPV) aircraft approach operation down to a 200 ft decision altitude (LPV200). Although the IUM may produce MMUs that are somewhat larger than the URAs previously envisioned for GPS IIIC, the analysis of the LPV200 operation indicates sufficiently high availability at U.S. locations, including Alaska and Hawaii. Analysis of several non-U.S. locations indicates availability values less than 0.99 and significant loss of availability in the Southern Hemisphere.

INTRODUCTION

Overview

The user range accuracy (URA) is a parameter in the GPS space vehicle (SV) broadcast message. Its purpose is to provide the means to calculate a bound for the errors in the SV signals-in-space (SIS). These errors include nominal (fault-free) and fault-induced ephemeris, clock[1] and signal distortion errors. In a user's receiver, URA is combined with standard deviations of other errors (e.g., user receiver errors and residual troposphere error) to estimate bounds on the ranging errors. These range error bounds are the inputs for the computation of an error bound for a user's position solution. For high integrity applications the position error needs to be bounded with high probability (on the order of $1 - 10^{-7}$).

GPS III, comprising Block III satellites and the next generation operational control system (OCX), is intended to have the potential to support such high integrity applications, without additional ground-based augmentation. A general discussion of the GPS III integrity concept may be found in [1]. For Block IIIA and IIIB satellites the level of integrity is intended to match the "legacy" level of $1 - 10^{-5}$ /h per SV for SIS. However, with Block IIIC satellites an "assured" integrity level of $1 - 10^{-8}$ / h per SV for SIS will be provided if the integrity status flag (ISF) is "on". Several methods for achieving such a high level of assured integrity are included in the GPS III integrity concept [1]. First, GPS III satellites will have the capability to detect clock faults or other on-board processing anomalies and rapidly switch the output signal to an untrackable non-standard code. Second, the OCX will take steps to assure that bad clock and ephemeris prediction data and URA data are not uploaded to a satellite. Of course the OCX will still also observe, estimate and correct slow drift satellite clock errors and ephemeris errors that may not be detectable by satellite on-board monitoring as is done by the current control segment.

The GPS III integrity concept as described in [1] is directed at addressing the two most significant integrity threats previously identified as satellite clock faults and bad data uploaded by the ground control system. However, there may be residual risks of other integrity failure modes that are large enough to require some additional mitigation. Furthermore, an independent SIS monitor may be needed, as in the FAA's Wide Area Augmentation System (WAAS), since approval authorities may not accept integrity parameters that are not independent of the process that generates the ephemeris and clock correction broadcast message.

[1] The SV broadcast data includes parameters for computing the SV clock correction. In this paper "clock error" refers to the residual clock error after application of the clock correction based on these broadcast parameters.

This paper examines the incorporation of an independent URA monitor (IUM) as one of the functions of the OCX that assures the broadcast URA bounds the ephemeris and clock errors according to the GPS IIIC assured integrity specification. The IUM does not monitor other SIS errors, such as signal distortion, which would require a separate monitor. The IUM is a process at the OCX that estimates ephemeris and clock errors independently from the OCX estimation process, using separate algorithms and computers, and possibly separate monitor receivers located at the OCX Monitor Stations (MSs). The method of error estimation is by least squares from single and multiple snapshot measurements. Since URA is an OCX generated upload parameter, it would be refreshed by the OCX every 15 min. Therefore, the IUM has to operate in the 15 min interval between OCX uploads.

The purpose of this paper is to illustrate the impact of an IUM on the magnitude of the broadcast URA and investigate the performance of GPS IIIC with an IUM, as part of the OCX, in meeting the integrity requirements of the Localizer Performance with Vertical Guidance (LPV) 200 (200 ft decision altitude) aircraft approach operation. Since LPV200 has stringent integrity requirements, the ability to satisfy these requirements provides an initial assessment of the operational feasibility of an IUM.

The IUM described herein is one approach to determining a high integrity URA. Other approaches, such as combining ground-based pseudorange measurements with space-based pseudorange measurements obtained through cross-link ranging, may provide additional improvements, but are beyond the scope of this study.

Contents

The rest of the paper is divided into the following five sections.

Description of IUM: This section contains the monitor process, including the minimum monitorable URA (MMU), the IUM's output for each SV when there is no threshold violation.

IUM Performance Model: This section includes the IUM measurement threshold definitions and assumptions used in the analysis.

MMU Results: This section contains MMU computations in both worldwide graphical and specific location tabular percentile formats.

Application to LPV200: The integrity availability of LPV200 is presented at representative U.S. locations and several selected worldwide locations.

Appendices: There are three appendices containing: A) assumed IUM measurement error model, B) fault-free ephemeris and clock error covariance model and C) an analysis of bounding the SV broadcast ephemeris and clock error distribution, including its dependence on a priori SV fault rate.

Some additional material on these topics may be found in [2].

DESCRIPTION OF IUM

IUM Overview

The objective of the IUM is to provide an independent check that 5.73 URA bounds an SV's ephemeris and clock broadcast errors with probability $1 - 10^{-8}$ per h with respect to fault-free and fault-induced errors. Figure 1 contains a flow chart of the IUM process.

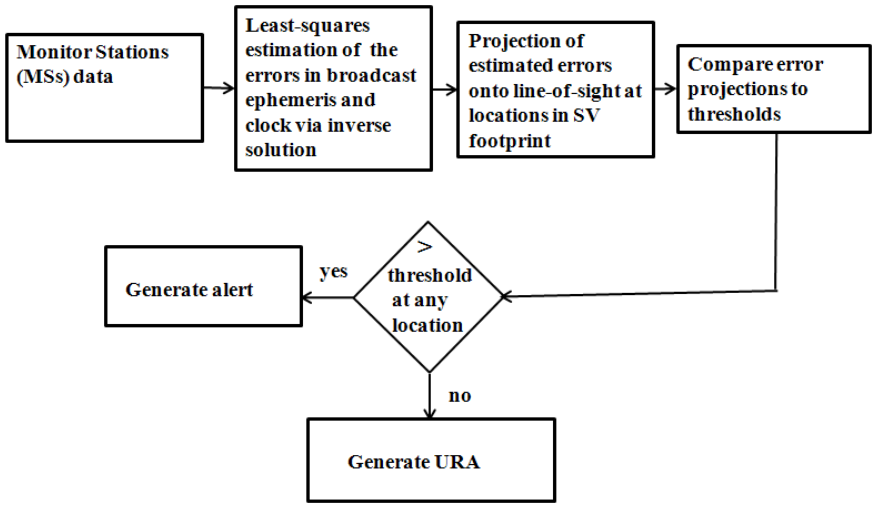

Figure 1. IUM Process

A range error estimate (δr_j) for each SV is formed as

$$\delta r_j = r_{j\_calc} - r_{j\_meas} \quad (1)$$

r_{j_calc}: calculated range based on SV broadcast ephemeris and exact location of MS_j

r_{j_meas}: measured range based on broadcast SV clock correction and MS clock (MS clocks are assumed to be perfectly synchronized)

The δr_j are the inputs to the SV position and clock error estimation solution (δ**e)** which is expressed as

$$\delta \mathbf{e} = \begin{bmatrix} \delta e_h \\ \delta e_c \\ \delta e_l \\ \delta e_t \end{bmatrix} = \begin{bmatrix} h_b \\ c_b \\ l_b \\ t_b \end{bmatrix} - \begin{bmatrix} \hat{h} \\ \hat{c} \\ \hat{l} \\ \hat{t} \end{bmatrix} \quad (2)$$

h_b, c_b, l_b, t_b : SV position and clock solution based on broadcast parameters coordinates

$\hat{h}, \hat{c}, \hat{l}, \hat{t}$: SV position and clock solution based on a weighted least squares solution using MS measurements and precise knowledge of MS antenna phase center coordinates

δ**e** is projected onto the line-of-sight at grid points in the SV footprint

$$\delta e_{i,k\_proj} = \mathbf{L}_{i,k}^{T} \bullet \delta \mathbf{e} \quad (3)$$

$\delta e_{i,k\_proj}$: decision statistic at location i, k

i, k: spherical angle grid coordinates

$\mathbf{L}_{i,k}$: line-of-sight unit vector from a grid point i, k in the SV footprint to the SV

$\delta e_{i,k\_proj}$ are the decision statistics that are compared to monitor threshold values ($T_{i,k}$) at the grid-points. If any $\delta e_{i,k\_proj} > T_{i,k}$, an alert is generated; otherwise a URA value is calculated for uplink to the SV for broadcast. The IUM computes a minimum monitorable URA (MMU). The uplinked URA for broadcast is URA ≥ max{URA_{pm}, MMU}, where URA_{pm} is the URA computed by the OCX prior to the monitor. The reason for the inequality is explained below.

Monitor Threshold

The threshold ($T_{i,k}$) is calculated at each grid point

$$T_{i,k} = k_T \sqrt{\sigma^2_{i,k\_meas} + \sigma^2_{i,k\_ure}} \tag{4}$$

k_T: threshold multiplier that sets false alert rate

σ_{i,k_meas}: standard deviation of the errors in IUM estimation of ephemeris and clock when projected onto grid coordinate line-of-sight

σ_{i,k_ure}: standard deviation of fault-free errors in SV ephemeris and clock broadcast (user range error (URE)) when projected onto grid coordinate line-of-sight

Note that $\sqrt{\sigma^2_{i,k\_meas} + \sigma^2_{i,k\_ure}}$ represents the decision statistic standard deviation at each grid point in the SV footprint in the absence of fault errors.

MMU Concept

MMU is the minimum value of URA for which the probability of loss of integrity given the presence of a fault (P_{LOIGF}) does not exceed a required value, P_{LOIGF_req}. That is,

$$P_{LOIGF} = \text{Prob}\{|\varepsilon_{act}| > 5.73\ \text{MMU} \mid \text{fault}\} \le P_{LOIGF\_req} \quad (5)$$

ε_{act}: component of user's actual range measurement error due to errors contained in the SV SIS (e.g, ephemeris and clock errors)

P_{LOIGF_req} is defined as

$$P_{LOIGF\_req} = \frac{P_{alloc}}{P_{fault}} \quad (6)$$

P_{alloc}: allocation per h for the risk of 5.73 URA not bounding URE due to a fault-induced error

P_{fault}: a priori probability of a fault per h. For example, if $P_{alloc} = 10^{-8}$ / h and $P_{fault} = 10^{-4}$ / h, $P_{LOIGF\_req} = 10^{-4}$.

Referring to (5), it is seen that if the pre-monitor URA computed by the OCX (URA_{pm}) were smaller than MMU then P_{LOIGF} could exceed P_{LOIGF_req}. However, for this IUM concept, MMU only reflects SV ephemeris and clock integrity. Therefore, URA_{pm} could be > MMU due to the OCX mitigating other fault modes, such as signal deformation. The assurance of the integrity of other fault modes is beyond the capability of this IUM since its decisions are based only on range measurements. Therefore, the broadcast URA would have to be

$$URA \geq \max\{URA_{pm}, MMU\} \quad (7)$$

MMU Definition

Two formulations of MMU have been defined. They are the monitor model formulation (MMU_{model}) and the protection level formulation (MMU_{PL}). The definitions and comparison of the two formulations are given below.

MMU_{model}

The following parameters are used in deriving MMU_{model}

m: measurement error contained in decision statistic in (3) at a grid point

σ_{meas}: standard deviation of m

e: fault-free SV broadcast error (ephemeris and clock) contained in decision statistic at a grid point

σ_{ure}: standard deviation of e

s = m + e: fault-free monitor test statistic

b: projection of fault-induced error in SV broadcast contained in decision statistic at a grid point

The location of the peak of a fault-induced error is unknown over the SV footprint. Therefore, the greatest risk of loss-of-integrity occurs at the maximum threshold location. MMU_{model} is computed at this location where $T_{max} = \max\{T_{i,k}\}$. Loss of integrity for a user at the same location as T_{max} is expressed as

$$|e + b| > K_I MMU \cap |s + b| \leq T_{max} \quad (8)$$

K_I: multiplier corresponding to required probability of loss of integrity

Assuming normal distributions of fault-free SV broadcast error e and IUM measurement error m, the probability of loss of integrity as a function of broadcast URA value U and fault-induced error b is

$$P_I(U,b) = \int_{K_I U - b}^{\infty} \int_{-T_{max}-b}^{T_{max}-b} f(s,e)\,ds\,de + \int_{-\infty}^{-K_I U - b} \int_{-T_{max}-b}^{T_{max}-b} f(s,e)\,ds\,de \tag{9}$$

where

$$f(s,e) = \frac{1}{2\pi\sqrt{\det(c)}} \exp\left(-0.5 \begin{bmatrix} s & e \end{bmatrix} c^{-1} \begin{bmatrix} s \\ e \end{bmatrix} \right) \tag{10}$$

$$c = \begin{bmatrix} \sigma_{meas}^2 + \sigma_{ure}^2 & \sigma_{ure}^2 \\ \sigma_{ure}^2 & \sigma_{ure}^2 \end{bmatrix} \tag{11}$$

$$MMU_{model} \text{ satisfies } \underset{b}{peak}\{P_I(MMU_{model}, b)\} = P_{LOIGF\_req} \tag{12}$$

Figure 2 shows the relationship between $P_I(U,b)$ and b given particular values of U, based on the error models in this paper and an arbitrary GPS/MSs geometry. In Figure 2, $P_{LOIGF_req} = 10^{-4}$is based on the assumptions that $P_{alloc} = 10^{-8}$ / h, $P_{fault} = 10^{-4}$ / h in (6). The figure shows that U = 0.823 m is the MMU for this P_{LOIGF_req} since peak{P_I (U > 0.823 m , b)} < 10^{-4} and peak{P_I (U < 0.823 m, b)} > 10^{-4}.

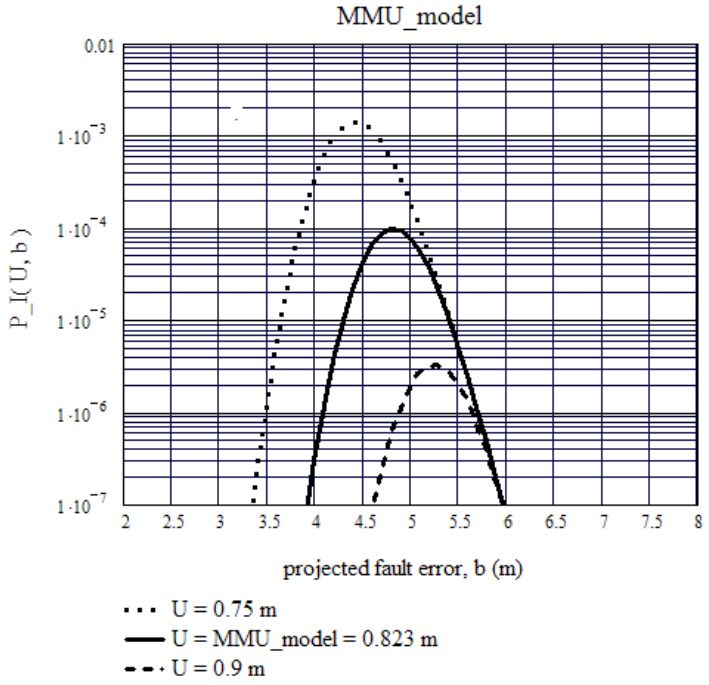

Figure 2. Illustration of MMU_{model} for the Case of $P_{LOIGF\_req} = 10^{-4}$

MMU_{PL}

MMU_{PL} is an intuitive and simpler definition of MMU. It is based on assuming that P_{LOIGF} equals the probability of missed detection (P_{md}). P_{md} is defined as the probability that the IUM measurement error hides a threshold violation.

$$P_{i,k\_md}(e+b) = \int_{-T_{i,k}-(e+b)}^{T_{i,k}-(e+b)} g(m)\,dm \tag{13}$$

$$g(m) = \frac{1}{\sqrt{2\pi}\,\sigma_{i,k\_meas}} \exp\left(-\frac{m^2}{2\,\sigma_{i,k\_meas}^2}\right) \tag{14}$$

The protection level bound is defined as

$$5.73\,\mathrm{MMU}_{i,k} \geq T_{i,k} + K_{md}\sigma_{i,k\_meas} \tag{15}$$

for all footprint locations.

$$\mathrm{MMU}_{PL} = \underset{i,k}{\mathrm{peak}}\left\{\frac{T_{i,k} + K_{md}\sigma_{i,k\_meas}}{5.73}\right\} \tag{16}$$

$$P_{md}\left(5.73\,\mathrm{MMU}_{PL}\right) = \int_{-T_{max}-5.73\,\mathrm{MMU}_{PL}}^{T_{max}-5.73\,\mathrm{MMU}_{PL}} g(m)\,dm \tag{17}$$

K_{md}: multiplier chosen via an iterative solution to make $P_{md}(5.73\,\mathrm{MMU}_{PL}) = P_{LOIGF\_req}$

Selection of URA Definition

Due to ease of MMU_{PL} computation and because $\mathrm{MMU}_{PL} \geq \mathrm{MMU}_{model}$, MMU_{PL} is chosen as the output of the IUM for implementation and IUM performance assessment. Referring to (9), proving that peak over b of $P_I(\mathrm{MMU}_{PL}, b) \leq P_{LOIGF\_req}$ is equivalent to proving that $\mathrm{MMU}_{PL} \geq \mathrm{MMU}_{model}$ for any given value of b.

$$P_I\left(\mathrm{MMU}_{PL}, b\right) = \int_{5.73\,\mathrm{MMU}_{PL}-b}^{\infty}\int_{-T_{max}-b}^{T_{max}-b} f(s,e)\,ds\,de + \int_{-\infty}^{-5.73\,\mathrm{MMU}_{PL}-b}\int_{-T_{max}-b}^{T_{max}-b} f(s,e)\,ds\,de \tag{18}$$

Since e and m are independent and the monitor decision statistic s = e + m

$$P_I\left(\mathrm{MMU}_{PL}, b\right) = \int_{5.73\,\mathrm{MMU}_{PL}-b}^{\infty}\int_{-T_{max}-(e+b)}^{T_{max}-(e+b)} g_e(e)\,g_m(m)\,dm\,de + \int_{-\infty}^{-5.73\,\mathrm{MMU}_{PL}-b}\int_{-T_{max}-(e+b)}^{T_{max}-(e+b)} g_e(e)\,g_m(m)\,dm\,de \tag{19}$$

The inner integral is the definition of $P_{md}(e+b)$ (13). The range of the first outer integral is $e \geq 5.73\ MMU_{PL} - b$ implying that $e+b \geq 5.73\ MMU_{PL}$. The range of the second outer integral is $e \leq -5.73\ MMU_{PL} - b$ implying that $e+b \leq -5.73\ MMU_{PL}$. Therefore, referring to (17), the inner integral in both cases is $\leq P_{LOIGF\_req}$ giving

$$P_I(MMU_{PL}, b) \leq P_{LOIGF\_req} \times \left[\int_{5.73MMU_{PL}-b}^{\infty} g_e(e)\,de \leq P_{LOIGF\_req} + \int_{-\infty}^{-5.73MMU_{PL}-b} g_e(e)\,de \leq P_{LOIGF\_req} \right] \leq P_{LOIGF\_req} \quad (20)$$

since

$$\int_{5.73MMU_{PL}-b}^{\infty} g_e(e)\,de + \int_{-\infty}^{-5.73MMU_{PL}-b} g_e(e)\,de \leq 1 \quad (21)$$

It was shown by several different examples that MMU_{PL} is also only slightly larger than MMU_{model} so that MMU_{PL} is a good approximation to the more rigorous MMU_{model}.

Since it has been shown that $P_I(MMU_{PL}, b) \leq P_{LOIGF\_req}$ then $5.73\ MMU_{PL}$ bounds any magnitude of fault error plus fault-free error plus any unknown inherent bias with risk $\leq P_{LOIGF\_req}$. The only assumptions made are the fault-free errors in the broadcast ephemeris and clock and the errors in the IUM measurements are normally distributed with 0 mean and MS clock synchronization error = 0.

Least Squares Estimate

Recursive least squares [3, p 33-35] is selected as the algorithm for combining a sequence of multiple snapshot range measurements into an independent solution of SV ephemeris and clock error. The least squares algorithm is chosen because it is not based on past orbital history or model, thus providing a completely independent estimation. Snapshot estimates are given by

$$\mathbf{E}_0 = \left(\mathbf{H}_0^{\mathrm{T}}\mathbf{W}_{\mathrm{meas},0}\mathbf{H}_0\right)^{-1}\mathbf{H}_0^{\mathrm{T}}\mathbf{W}_{\mathrm{meas},0}\delta\mathbf{r}_0$$

(one snapshot) (22)

$$\mathbf{E}_{q+1} = \mathbf{E}_q + \mathbf{K}_{q+1}\left(\delta\mathbf{r}_{q+1} - \mathbf{H}_{q+1}\mathbf{E}_q\right)$$

(multiple snapshots) (23)

E: estimate of the errors in the SV broadcast ephemeris and clock

q: update index

K: gain

$\delta\mathbf{r}$: range measurement error vector defined in (1)

H: measurement matrix for SV position and clock error solution

$\mathbf{W}_{\mathrm{meas}}$: diagonal weight matrix representing the monitor receiver measurement errors (inverse of measurement error variances)

The covariance matrix (**cov**) of the SV ephemeris and clock error solution is given by

$$\mathbf{cov}_0 = \left(\mathbf{H}_0^{\mathrm{T}}\mathbf{W}_{\mathrm{meas},0}\mathbf{H}_0\right)^{-1} \quad (24)$$

$$\mathbf{S}_{q+1} = \mathbf{H}_{q+1}\mathbf{cov}_q\mathbf{H}_{q+1}^{\mathrm{T}} + \mathbf{W}_{\mathrm{meas},q+1}^{-1} \quad (25)$$

$$\mathbf{K}_{q+1} = \mathbf{cov}_q - \mathbf{H}_{q+1}^{\mathrm{T}}\mathbf{S}_{q+1}^{-1} \quad (26)$$

$$\mathbf{cov}_{q+1} = \mathbf{cov}_{q} - \mathbf{K}_{q+1}\mathbf{S}_{q+1}\mathbf{K}_{q+1}^{T} \tag{27}$$

The above recursive least squares equations can be implemented in either Earth-Centered, Earth-Fixed (ECEF) or satellite Height, Cross-Track, Along-Track (HCLT) coordinate frame. The algorithm is implemented in HCLT in the model used for analysis because it is more reasonable to assume that the errors to be estimated by the recursive least squares remain constant in HCLT frame rather than in the ECEF frame. The conversion of **E**, **H** and **cov** between ECEF and HCLT are

$$\mathbf{E}_{ECEF} = \mathbf{M}\mathbf{E}_{HCLT} \tag{28}$$

$$\mathbf{H}_{ECEF} = \mathbf{H}_{HCLT}\mathbf{M}^{T} \tag{29}$$

$$\mathbf{cov}_{ECEF} = \mathbf{M}\mathbf{cov}_{HCLT}\mathbf{M}^{T} \tag{30}$$

Where the mapping matrix **M** is a 4x4 matrix constructed as

$$\mathbf{M} = \begin{bmatrix} \mathbf{h}_{ECEF,3x1} & \mathbf{c}_{ECEF,3x1} & \mathbf{l}_{ECEF,3x1} & \mathbf{0}_{3x1} \\ 0 & 0 & 0 & 1 \end{bmatrix} \tag{31}$$

Where $\mathbf{h}_{ECEF,3x1}, \mathbf{c}_{ECEF,3x1}, \mathbf{l}_{ECEF,3x1}$ are the unit vectors of the axes of the satellite HCLT coordinate frame represented in the ECEF coordinate frame.

Assumed $\mathbf{W}_{meas}$

$\mathbf{W}_{meas}$ is a parameter of (22), (24) and (25). It is a diagonal matrix with elements along the diagonal calculated as

$$W_{i,i\_meas}(t_i, el_i) = \left[\sigma^2_{cnmp}(t_i) + \sigma^2_{tropo}(el_i) + \sigma^2_{clock}\right]^{-1} \quad (32)$$

t_i: elapsed time since SV acquisition

el_i: elevation angle from MS to SV

i: monitor station index

σ_{cnmp}: standard deviation of errors due to monitor receiver code and multipath noise sources, a function of time (t_i) since acquisition

σ_{tropo}: standard deviation of errors due to un-modeled troposphere delay, a function of elevation angle (el_i) to the SV

σ_{clock}: standard deviation of monitor receiver clock synchronization error (monitor clocks are assumed to be synchronized)

The equations for σ_{cnmp} and σ_{tropo} are defined in Appendix A. σ_{clock} is assumed = 0 for this performance analysis.

Measurement Process

The measurement process is a sliding window to account for pop-up fault errors that could occur at any time. The snapshot measurements of an SV are separated by $\Delta\tau$. $\Delta\tau$ is the minimum interval between independent measurements. $\Delta\tau$ is determined by the measurement error correlation time due to multipath and estimator smoothing. In this study it is assumed that $\Delta\tau$ = 5 min. The SV broadcast ephemeris and clock correction data are assumed to be updated by the OCX every 15 min.

For monitoring URA prior to upload, four sets of snapshots could be processed during each 15 min interval between SV updates:

4 snapshots at $\tau = 0^+$, 5, 10, 15^- min

3 snapshots at $\tau = 5, 10, 15^-$

2 snapshots at $\tau = 10, 15^-$

1 snapshot at $\tau = 15^-$

0^+: start time of new upload interval

15^-: maximum time to make URA decision

In practice, to account for a fault-induced error occurring after 10 min, integrity credit with respect to monitoring URA may only be given for the one snapshot MMU at 15^- min. For example, assume that a fault error occurs after 10 min and is just above the threshold for a single snapshot decision. However, in the four snapshot decision at 15^- min (0^+, 5, 10 15^-) that same fault error would be diluted by ≅ 1/4 in the decision statistic while the threshold would be decreased by ≅ 1/2 so that the error might not be detected.

IUM PERFORMANCE MODEL

MMU_{PL} Parameters

The computation of MMU_{PL} requires four parameters (16). The threshold component requires three parameters (4): k_T, $\sigma_{i,\ k\_meas}$, and $\sigma_{i,\ k\_ure}$. The fourth parameter is K_{md}.

k_T

k_T sets the false detection probability (P_{fd}). For this analysis, the target false detection probability (P_{fd}) per decision is based on the assumption that it is desired to limit the false detection rate to 1 / year per SV. Since the SV URA update occurs every 15 min there are 4 URA decisions / h.

$$P_{fd} = (365 \times 24 \times 4)^{-1} = 2.85 \times 10^{-5} \quad (33)$$

The test statistics at sample locations in the SV footprint are not independent because they are linear combinations of the clock and three ephemeris error components (3). Therefore, the analytical derivation of k_T is complicated. An estimate of k_T was derived by Monte Carlo simulations of the fault-free threshold comparison process for an example of good snapshot geometry (relatively small MMU) from a model GPS III constellation and various numbers of grid points, as illustrated in Figure 3. The grid points were evenly spaced for each of the spherical coordinate angles within the footprint. For example, for 900 grid points the layout was 0, 4…76° (zenith angle) and 0, 8…352° (azimuth) which yields 20 × 45 = 900 grid points.

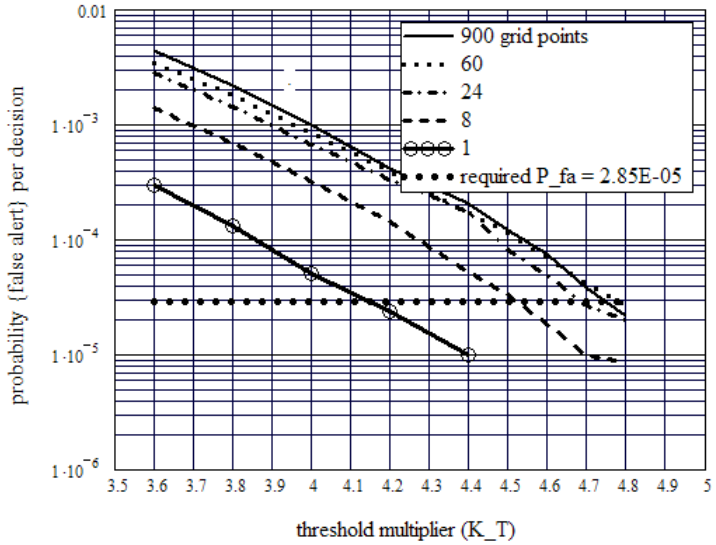

Figure 3 Results of Derivation of k_T Via Simulation

As shown in the figure as the number of grid points increases, P_{fd} as a function of k_T converges to a single graph that is assumed to be represented by the 60 grid points graph. The intersection of each graph with the 2.85×10^{-5} line provides an estimate of k_T for that particular number of grid points. Therefore the intersection of the 60 points graph indicates the estimate of k_T for this snapshot is 4.8. Since the purpose of the threshold test is to detect fault induced errors it is desirable to have as many grid points as is practical to ensure that the SV footprint is sufficiently sampled. Since the k_T estimate is based on convergence, $k_T = 4.8$ would be valid for good geometry cases for any number of grid points greater than 60. For

example, assume the grid spacing is 1° for both spherical angle coordinates then the number of grid points would be 77 × 360 = 27,720. If the statistics at each grid point were assumed for convenience to be independent as in [2] then $k_T = 6.11$, which would be too large a value. A similar simulation was performed for an example of poor snapshot geometry (large MMU) from the GPS III model constellation. The resulting estimate was $k_T = 5$. The subsequent results in this paper assume $k_T = 5$.

$\sigma_{i,\,k\_meas}$

Referring to (30)

$$\sigma_{i,\,k\_meas} = \sqrt{\mathbf{L}_{i,\,k}^{T}\ \mathbf{cov}\,\mathbf{L}_{i,\,k}} \tag{34}$$

$\sigma_{i,\,k\_ure}$

An assumed covariance matrix of the fault-free errors in the ephemeris and clock correction broadcast ($\mathbf{C}_{ure}$) is needed to calculate σ_{ure}. An analysis of actual GPS data was performed in order to assemble a typical covariance ($\mathbf{C}_{typ}$) that is based on broadcast ephemeris and clock correction data and precise ephemeris and clock correction data from a present GPS SV. The data for formulating $\mathbf{C}_{typ}$ was processed from data obtained from the NGA website for a typical SV, as described in Appendix B.

$$\mathbf{C}_{typ} = \begin{bmatrix} 0.0608 & -0.0104 & -0.0820 & 0.2724 \\ -0.0104 & 0.2216 & -0.2415 & -0.0495 \\ -0.0820 & -0.2415 & 0.9456 & -0.4499 \\ 0.2724 & -0.0495 & -0.4499 & 1.5495 \end{bmatrix} \text{ in HCLT coordinates} \tag{35}$$

A GPS IIIC era ephemeris and clock RMS error over the SV footprint is assumed to be $\sigma_{ure} = 0.25$ m. Using an equation derived in [4, p 598], this RMS value is satisfied by finding a multiplier, a, such that

$$\sigma_{ure} = a\sqrt{\frac{1}{49}\left[\left(\mathbf{C}_{typ}\right)_{2,2} + \left(\mathbf{C}_{typ}\right)_{3,3}\right] + 0.959\left(\mathbf{C}_{typ}\right)_{1,1} + \left(\mathbf{C}_{typ}\right)_{1,4} + 1.959\left(\mathbf{C}_{typ}\right)_{4,4}} = 0.25\,\text{m} \tag{36}$$

$$a = 0.1699 \tag{37}$$

The assumed $\mathbf{C}_{ure} = a^2\,\mathbf{C}_{typ}$

$$\mathbf{C}_{ure} = \begin{bmatrix} 0.1754 & -0.0299 & -0.2366 & 0.7864 \\ -0.0299 & 0.6395 & -0.6972 & -0.1428 \\ -0.2366 & -0.6972 & 2.7295 & -1.2986 \\ 0.7864 & -0.1428 & -1.2986 & 4.4725 \end{bmatrix} \times 10^{-2} \tag{38}$$

$$\sigma_{i,k\_ure} = \sqrt{\mathbf{L}_{i,k}^{T}\,\mathbf{C}_{ure}\,\mathbf{L}_{i,k}} \tag{39}$$

K_{md}

K_{md} is contained and defined in the MMU_{PL} equations (15 - 17). Assuming $P_{md} = 10^{-4}$, $K_{md} = 3.72$.

MMU RESULTS

This section summarizes the MMU results obtained from the performance model for one snapshot and up to four snapshots. Up to four snapshots means that within any 15 minute interval, the number of snapshots processed is up to 4, depending on the number of 5-minute time steps for which at least 4 MSs were in view of the satellite. The analysis relies on the same network of 17 MSs currently used by the GPS control segment.

Assumed Monitor Receiver Elevation Angle Mask

To illustrate IUM global coverage sensitivity to the selection of elevation mask angle, global MMU results assuming 10° mask angle for USAF and 15° mask angle for NGA monitor stations are first presented. Thereafter, the selected mask angle for the IUM is 5° for all of the MSs, the value used in the FAA's Wide Area Augmentation System (WAAS).

Worldwide MMU results

Figures 4 and 5 contain graphical overviews of worldwide MMU values assuming 10° and 15° IUM elevation angle masks and 5° IUM elevation angle masks, respectively. The small dots indicate $MMU_{PL} \leq 1$m, large dots 1 m $\leq MMU_{PL} \leq 2$ m and the solid lines $MMU_{PL} > 2$ m. The unmonitored results are indicated by the circles in the SV traces. The dots correspond to 5 min time steps. Unmonitored SV means that less than 4 MS view the SV. Based on the data of Figure 4, the percent of unmonitored SVs is 22.6% for the assumed 10°, 15° elevation angle masks. Referring to Figure 5, the percent of unmonitored SVs obtained assuming a 5° elevation mask angle is 2.8%.

Figure 6 contains the worldwide MMU results for up to four snapshots and 5° IUM mask angle. The interval between dots corresponds to a 15 min time step.

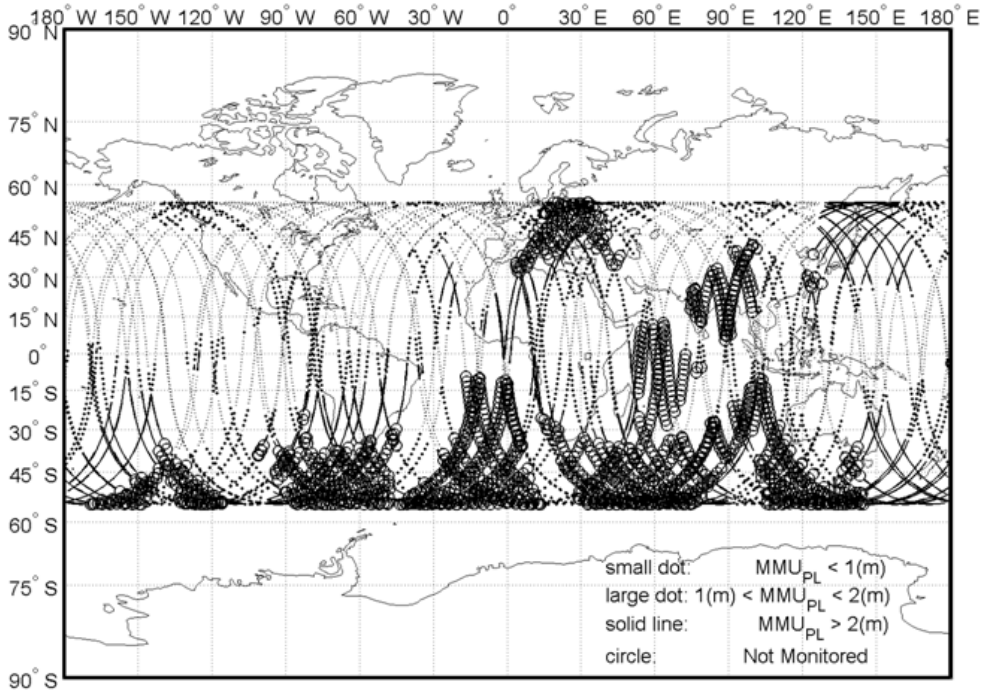

Figure 4. GPS III SV Ground Tracks With MMU_{PL} Values:

One Snapshot, Monitor Elevation Mask Angles 10° (USAF), 15° (NGA)

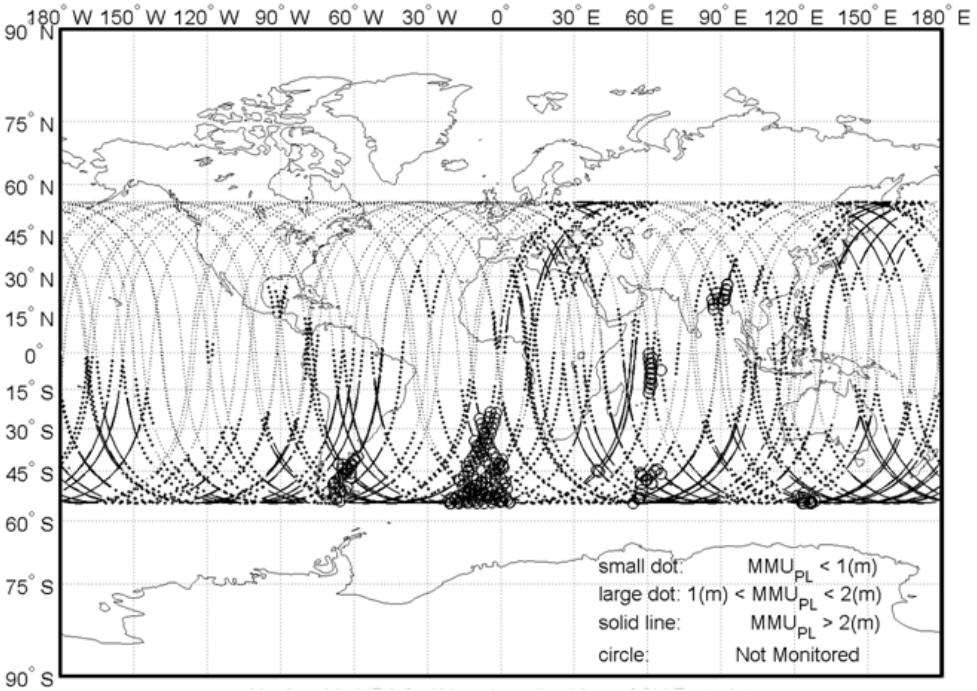

Figure 5. GPS III SV Ground Tracks With MMU_{PL} Values:

One Snapshot, All Monitor Elevation Mask Angles = 5°

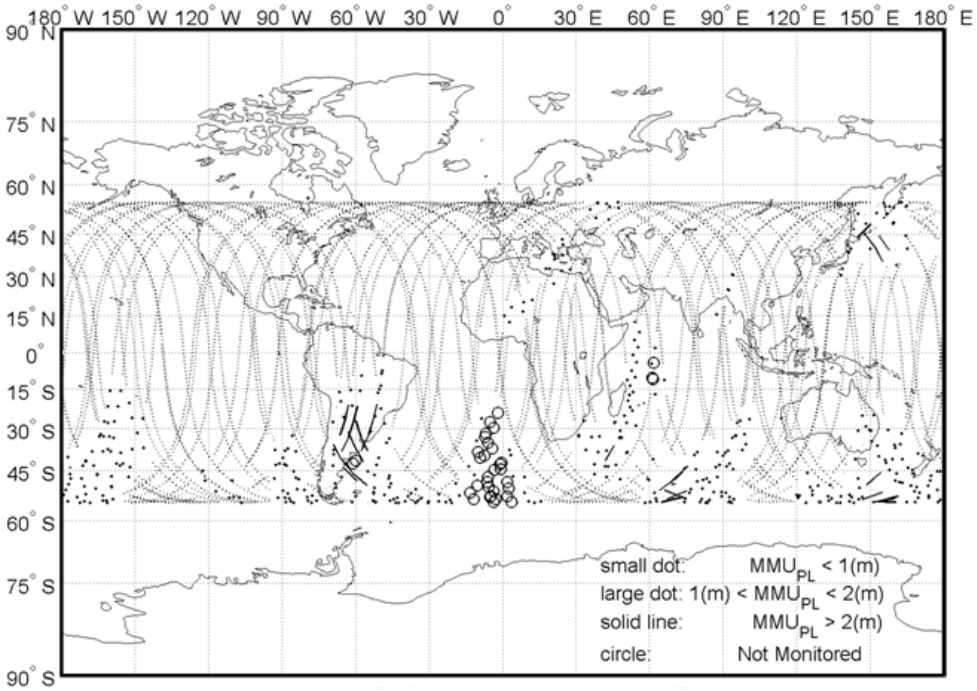

Figure 6. GPS III SV Ground Tracks With MMU_{PL} Values:

UP To Four Snapshots, All Monitor Elevation Mask Angles = 5°

Table 1 compares worldwide percentiles for one snapshot and up to four snapshot MMUs. Compared to one snapshot, up to four snapshots would yield significantly smaller values of MMU.

Table 1. Worldwide MMU Percentiles

%-tile	1 snapshot (m)	Up to 4 snapshots (m)
0	0.52	0.31
20	0.72	0.40
30	0.80	0.44
40	0.90	0.48
50	1.0	0.55
60	1.25	0.65
70	1.57	0.78
80	1.96	0.98
90	2.78	1.36
95	3.86	1.80
maximum	1199	232

MMU Results at Specific Locations

U. S. Locations

One snapshot MMU percentiles at eight U.S. city locations (locations of major airports) are displayed in Table 2. For these locations MMU values beyond ≅ 40 %-tile, are greater than the desired value of integrity assured URA ≤ 0.7 m for GPS IIIC. Median values are approximately 0.7 – 0.8 m.

Table 2. U.S. Locations: MMU Computed From One Snapshot

%-tile and other statistics	Seattle (m)	San Diego (m)	Minn./ St. Paul (m)	Houston (m)	Boston (m)	Miami (m)	Juneau (m)	Honolulu (m)
0 %	0.522	0.522	0.530	0.530	0.530	0.530	0522	0.522
20	0.627	0.628	0.637	0.638	0.647	0.646	0.630	0.631
40	0.700	0.706	0.710	0.709	0.722	0.716	0.714	0.732
50	0.734	0.748	0.747	0.743	0.765	0.753	0.761	0.795
60	0.784	0.795	0.791	0.793	0.814	0.802	0.812	0.869
80	0.956	1.019	0.947	0.964	1.032	0.993	1.007	1.350
90	1.271	1.383	1.185	1.256	1.426	1.464	1.390	2.087
95	2.043	1.951	1.699	1.755	2.256	2.699	2.218	2.918
99	12.975	11.941	3.467	8.751	5.271	25.266	12.305	12.975

maxi-mum	769.2	769.2	7.92	34.263	19.360	1199	769.2	769.2
% un-mon	0	0	0	0	0	0.241	0	0
no. of samples	2523	2507	2489	2487	2457	2483	2718	2531

Comparison of One and Up To Four Snapshot Derived MMUs

Table 3 contains a comparison between median MMU values based on one snapshot and four snapshots. There is an approximate 50% reduction in MMU magnitude when four snapshots are used as compared with one snapshot. An MMU based on four snapshots is more likely to meet the desired URA ≤ 0.7 m. However, as noted previously, multi-snapshot estimates may not detect a fault error occurring toward the end of a recursion interval so that only a one snapshot MMU may be acceptable.

Table 3. Comparison of Median Values of MMUs Based on One and Four Snapshots

Location	Median MMU_PL 1 snapshot (m)	Median MMU_PL up to 4 snapshots (m)	Ratio MMU_PL(up to 4 snap.) / MMU_PL(1 snap.)
Seattle	0.734	0.404	0.550
San Diego	0.748	0.410	0.548

Minn. / St. Paul	0.747	0.408	0.546
Houston	0.743	0.407	0.548
Boston	0.765	0.417	0.545
Miami	0.753	0.410	0.545
Juneau	0.761	0.415	0.545
Honolulu	0.795	0.435	0.547
London	0.834	0.446	0.535
Frankfort	0.844	0.454	0.538
Moscow	0.889	0.470	0.529
Beijing	0.905	0.481	0.531
Tokyo	0.871	0.466	0.535
Rio de Janeiro	1.221	0.626	0.513
Buenos Aires	1.226	0.632	0.515
Cape Town	1.536	0.780	0.508
Sydney	1.343	0.688	0.512
Wellington	1.536	0.752	0.490

MMU Variation

MMU varies over time with SV motion. The variation depends upon the number of monitor stations that can observe the SV above the elevation mask angle and the geometry of the error projection onto the location with the maximum monitor threshold (T_{max}). Figure 7 contains example variations over 24 h for MMUs based on one and up to four snapshots. The MMUs based on up to four snapshots are generally significantly reduced in comparison to MMUs based on one snapshot. Typical ratios of MMU derived from up to four snapshots to those derived from one snapshot range from 0.4 to 0.6. However, during periods of extremely poor geometries, the ratio can be somewhat larger or smaller than the typical value. If the four snapshot algorithm can actually use only a single snapshot, the ratio becomes 1.0. If the four snapshot algorithm can use additional geometries to smooth out the effect of the poor geometry on the one-snapshot algorithm, then the ratio can be as small as 0.2.

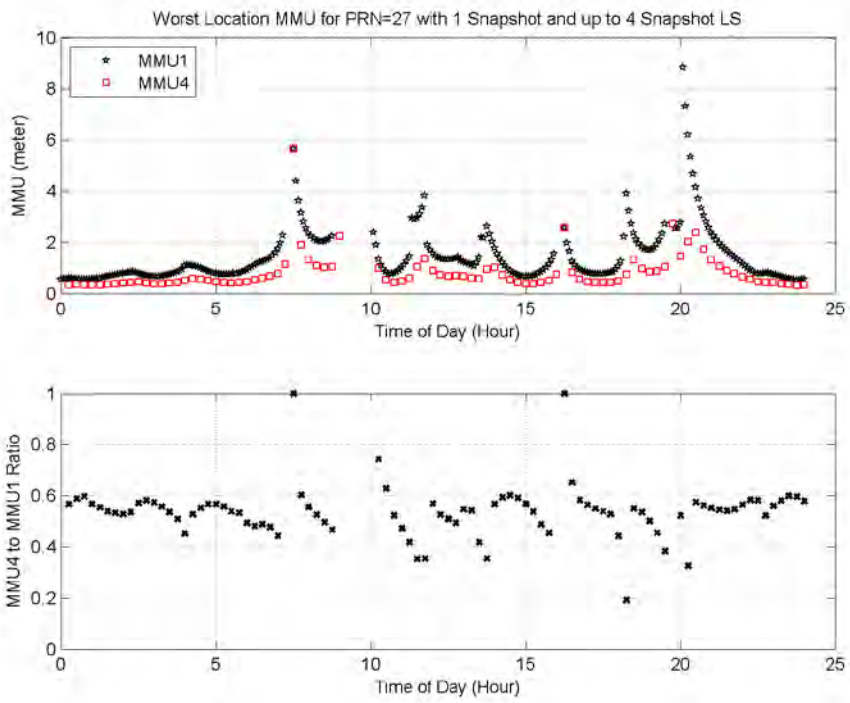

Figure 7. Example MMU Variation Versus Time Along SV Track

APPLICATION to LPV200

User Error Model

Error Equations

In addition to an MMU serving to bound SIS errors, the LPV200 application requires an airborne user receiver error model since the navigation sensor error (NSE) includes both SIS and user receiver measurement errors. The user based errors are assumed to be due to receiver noise, multipath noise and residual troposphere error, characterized by σ_{rn}, σ_{mp} and σ_{tropo}, respectively. The standard deviation equations are from [5] for single frequency errors.

The total user dual-frequency range measurement error standard deviation for SV_j is

$$\sigma_{tot}(el_u) = \sqrt{MMU_u^2 + \sigma_{rnmp}^2(el_u) + \sigma_{tropo}^2(el_u)} \tag{40}$$

$$\sigma_{rnmp}{}^2(el_u) = d^2\left[\sigma_{mp}^2(el_u) + \sigma_{rn}^2(el_u)\right] \tag{41}$$

u: SV index

d: dual-frequency error multiplication factor = 2.59 for L1 and L5

The diagonal elements of the user position solution integrity weight matrix ($\mathbf{W}_I$) are given by

$$W_{u,u\_I} = \sigma_{tot}^{-2}(el_u) \tag{42}$$

The user position solution limits are assumed to be elevation angle ≥ 5° and MMU ≤ 10 m.

Over Bound

The vertical requirements for LPV200 are significantly more difficult to achieve than the horizontal requirements. Therefore, their achievement usually also implies achievement of horizontal requirements. All of the LPV200 application results are based on the root-sum-square (RSS) of the projections of the $\sigma_{tot}(el_u)$ onto the user's vertical position direction.

$$\sigma_{vert} = \sqrt{\sum_{j=1}^{N} S_{3,u}^2 \, \sigma_{tot}^2 \left(el_u\right)} \tag{43}$$

$S_{3,u}$: solution vertical projection coefficient for SV_u

N: number of SVs in solution

For σ_{vert} to be used in satisfying the integrity of the position solution, each $\sigma_{tot}(el_u)$ has to be the standard deviation that characterizes a normal distribution, $N\{0, \sigma_{tot}^2 \left(el_u\right)\}$, that over bounds the distribution of the user's total range error for each SV_u, as proven in [6]. Based on an analysis in [7], Appendix C contains a definition and analysis of an over bounding concept where multiples of MMU are the bounds on the SIS component of the total user range error. The appendix illustrates that over bounding is achieved for the SIS errors for this application when $P_{fault} \leq 10^{-3}$ / h, $P_{LOIGF\_req} = P_{alloc} / P_{fault} = 10^{-8} / P_{fault}$.

LPV200 Requirements

There are four NSE vertical requirements that need to be satisfied for LPV200 as identified in [7]. It is noted that there is also a 6 s integrity response time that is not addressed by the IUM since the OCX updates are every 15 min. The 6 s response time would conceptually be addressed by an on-board SV monitor. The four requirements are presented below.

Fault-Present Vertical Requirements

- Vertical protection level (VPL) ≤ 35 m

- $\text{Prob}\{\text{NSE}|_{\text{fault present}} \leq 15 \text{ m}\} \geq 1 - 10^{-5}$

Fault-Free Vertical Requirements

- $\text{Prob}\{\text{NSE}|_{\text{fault free}} \leq 4 \text{ m}\} \geq 0.95$

- $\text{Prob}\{\text{NSE}|_{\text{fault free}} \leq 10 \text{ m}\} \geq 1 - 10^{-7}$

Performance Measure

Availability of service is a standard performance measure when assessing the operational feasibility of an integrity concept. The availability models that are described assume that the full constellation of 27 SVs is in operation (no SV outages). A more rigorous availability model would account for SV outages. Therefore, the availability results are slightly optimistic.

Vertical Protection Level (VPL) Availability

$$\mathbf{C}_{\text{I}} = \left(\mathbf{H}_{\text{user}}^{\text{T}} \, \mathbf{W}_{\text{I}} \mathbf{H}_{\text{user}}\right)^{-1} \tag{44}$$

$$\text{VPL} = \text{K}_{\text{VPL}} \sqrt{\left(\mathbf{C}_{\text{I}}\right)_{3,3}} \tag{45}$$

$\mathbf{H}_{\text{user}}$: user measurement matrix

$\mathbf{C}_{\text{I}}$: covariance matrix containing integrity weight $\mathbf{W}_{\text{I}}$

$$\sqrt{\left(\mathbf{C}_{\text{I}}\right)_{3,3}} = \sigma_{\text{vert}} \tag{46}$$

K_{VPL}: VPL multiplier = 5.33 (corresponds to WAAS LPV200)

$$\text{avail}_{\text{VPL}} = \frac{\text{no.}\left(\text{VPL} \le 35\,\text{m}\right)}{\text{N}} \tag{47}$$

N: no. of samples = 288 per location (sampling interval = 5 min over 24 h)

NSE Fault-Present Availability

$$\text{NSE}\big|_{\text{fault present}} = 4.42\sqrt{\left(\mathbf{C}_{\text{I}}\right)_{3,3}} \tag{48}$$

$$(4.42 \text{ corresponds to probability} = 1\text{-}10^{-5})$$

$$\text{avail}_{\text{fault present}} = \frac{\text{no.}\left(\text{NSE}\big|_{\text{fault present}} \le 15\,\text{m}\right)}{\text{N}} \tag{49}$$

NSE Fault-Free Availability

The position solution uses integrity weight matrix $\mathbf{W}_{\text{I}}$ that is based on MMU, but the fault-free component in the total range error variance has to be represented by σ^2_{ure} rather than MMU. Define

$$\text{W}_{\text{u, u\_ff}} = \left[\sigma^2_{\text{ure}} + \sigma^2_{\text{rnmp}}\left(\text{el}_{\text{u}}\right) + \sigma^2_{\text{tropo}}\left(\text{el}_{\text{u}}\right)\right]^{-1} \tag{50}$$

σ_{ure} = 0.3 m (51)

$$\mathbf{s} = \left(\mathbf{H}^{\text{T}}\ \mathbf{W}_{\text{I}}\ \mathbf{H}\right)^{-1}\mathbf{H}^{\text{T}}\ \mathbf{W}_{\text{I}} \tag{52}$$

The fault-free error covariance is

$$\mathbf{C}_{\mathrm{ff}} = \mathbf{s}\,\mathbf{W}_{\mathbf{ff}}^{-1}\,\mathbf{s}^{\mathbf{T}} \tag{53}$$

$$\mathrm{avail}_{\mathrm{ff}}\left(\mathrm{K}_{\mathrm{ff}}, \mathrm{V}\right) = \frac{\mathrm{no.}\left(\mathrm{K}_{\mathrm{ff}}\sqrt{\left(\mathbf{C}_{\mathrm{ff}}\right)_{3,3}} \le \mathrm{V}\right)}{\mathrm{N}} \tag{54}$$

$$\mathrm{avail}_{\mathrm{fault\ free}}\big|_{\mathrm{NSE} \le 4\,\mathrm{m}} = \mathrm{avail}_{\mathrm{ff}}\left(1.96, 4\,\mathrm{m}\right)$$
$$(1.96\ \text{corresponds to prob.} = 0.95) \tag{55}$$

$$\mathrm{avail}_{\mathrm{fault\ free}}\big|_{\mathrm{NSE} \le 10\,\mathrm{m}} = \mathrm{avail}_{\mathrm{ff}}\left(5.33, 10\,\mathrm{m}\right)$$
$$(5.33\ \text{corresponds to prob.} = 1\text{-}10^{-7}) \tag{56}$$

The achieved availability is the fraction of the number of time steps (N_{sat}) where all four availability requirements are satisfied

$$\mathrm{avail}_{\mathrm{achiev}} = \frac{\mathrm{N}_{\mathrm{sat}}}{288} \tag{57}$$

Availability Results

U.S. Locations

Availability results for the sample U.S. locations are contained in Table 4. As stated previously the availability values are based on no SV outages. It is seen that most achieved availabilities are 1 and the lowest availability (0.993) occurs at Juneau.

Table 4. Availability at U.S. Locations (No SV Outages, All-In-View, One Snapshot MMU)

location	avail fault error VPL ≤ 35 m	avail fault present NSE ≤ 15 m	avail fault free NSE ≤ 4 m	avail fault free NSE ≤10 m	achieved availability
Seattle	1	1	1	1	1
San Diego	1	1	1	0.997	0.997
Minneapolis St. Paul	1	1	1	1	1
Houston	1	1	1	0.997	0.997
Boston	1	1	1	1	1
Miami	1	1	1	1	1
Juneau	1	1	0.997	0.993	0.993
Honolulu	1	1	1	1	1

Non-U.S. Locations

Availability results for the sample non-U.S. locations are contained in Table 5. Except for London, Frankfort and Beijing, the availability results are ≤ 0.983. It is noted that it is desirable to achieve availability greater than 0.99 for LPV200 operation.

Table 5. Availability at non-U.S. Locations (No SV Outages, All-In-View, One Snapshot MMU)

location	avail fault error VPL ≤ 35 m	avail fault present NSE ≤ 15 m	avail fault free NSE ≤ 4 m	avail fault free NSE ≤10 m	achieved availability
London	1	1	1	1	1
Frankfort	1	1	1	1	1
Moscow	1	1	0.997	0.983	0.983
Beijing	1	1	1	1	1
Tokyo	1	0.993	0.993	0.969	0.969
Rio de Janeiro	1	0.917	0.944	0.906	0.878
Buenos Aires	0.983	0.806	0.858	0.816	0.750
Cape Town	0.997	0.757	0.931	0.878	0.726
Sydney	1	0.778	0.986	0.934	0.757
Wellington	0.993	0.778	0.962	0.944	0.764
North Pole	1	1	0.976	0.941	0.941
South Pole	0.969	0.323	0.726	0.545	0.257

SUMMARY OF RESULTS AND LIMITATIONS

1. If the broadcast URA ≥ minimum monitorable URA (MMU) as defined in this paper, the GPS IIIC SV signal-in-space 5.73 URA error bound for $\leq 10^{-8}$ integrity risk would be assured for any ephemeris and clock error type (fault-free or fault-induced), provided that the SV fault error rate $\leq 10^{-3}$ / h.

2. The monitor receiver elevation mask angle should be no greater than 5° for effective coverage for independent SV position determination

3. For U.S. locations, the median and 95%-tile MMU values are approximately 0.75 – 0.8 m and 2 – 3 m, respectively (given the assumptions of the analysis).

4. For the non-U.S. locations considered, the median and 95% MMU values are approximately 0.8 – 1.5 m and 2 – 6 m, respectively (given the assumptions of the analysis).

5. The MMU values are generally greater than the GPS IIIC maximum specified URA broadcast value (0.7 m) (given the assumptions of the analysis). Therefore, if IUM were part of the OCX for GPS IIIC then the broadcast URA would usually be > 0.7 m.

6. Although IUM would not support a broadcast URA ≤ 0.7 m, it would still provide high availability for the stringent requirements of LPV200 approaches at U.S. airports. For all U.S. major airports considered, achieved availability ≥ 0.997 except for Juneau (0.993). However, LPV200 availability at the ten non-U.S. airports considered for analysis ranged between 0.75 – 1, with the degraded availability being most prominent in the southern hemisphere.

7. The main limitations of the IUM presented herein:

    - IUM SV position determination is based on one snapshot. If SV position accuracy were enhanced by multiple snapshots, smaller values of MMU could be achieved. However, it would be more difficult to detect a fault error that occurred after the start of a measurement window since the fault error would be diluted to a greater extent than the threshold was lowered.

- Since only one integrity parameter (URA) is broadcast, MMU has to be the peak value over the SV footprint in order to assure integrity at the worst user location in the SV footprint.

The contents of this material reflect the views of the authors and/or the Director of the Center for Advanced Aviation System Development of The MITRE Corporation. Neither the Federal Aviation Administration nor the Department of Transportation makes any warranty or guarantee, or promise, expressed or implied, concerning the content or accuracy of the views expressed herein. Approved for Public Release:10-4468. Distribution Unlimited.

REFERENCES

1. Kovach, K., J. Dobyne, M. Crews and C. Miles, "GPS III Integrity Concept", *Proceedings of ION GNSS 2008*, Sept. 2008.

2. Braff, R., B. Bian and C. Shively, *Independent Control Segment URA Monitor for GPS IIIC with Application to LPV200*, MITRE Corporation, (to be published).
3. Bar-Sholom, Y., Fortmann, T.E., *Tracking and Data Asso*ciation, Academic Press, 1988.

4. Zuberge, J. F. and Bertiger, W.I., *Ephemeris and Clock Navigation Message Accuracy*, *Global Positioning System: Theory and Applications*, Vol. 1, AIAA, 1996.

5. RTCA SC-159, *Minimum Operational Performance Standards for Global Positioning System / Wide Area Augmentation System Airborne Equipment*, RTCA DO-229D, December 13, 2006.

6. DeCleene, B., "Defining Pseudorange Integrity Over Bounding", *Proceedings of ION GPS 2000*, September 2000.

7. Shively, C., "Analysis of Specified and Hypothetical GPS IIIC Integrity for LPV200 Operations", *Proceedings of ION 2010 International Technical Meeting*, January 2010.

8. MS receiver accuracy model is based on Shallberg, K. and Ericson, S. (private communication), *CNMP Considerations for Future Ground Stations*, GREI / Zeta Associates report, 6/12/2007.

APPENDIX A: MS MEASUREMENT ERROR MODELS

MS Receiver Error

The MS receiver errors are characterized by an error equation derived from the testing of an advanced monitor receiver [8]. The error equation models code noise and multipath noise (CNMP) as function of time (t) since an SV was acquired by the receiver.

$$\sigma_{CNMP} = \frac{Mean\_Error(t)}{K_{CNMP}} + \sigma_{carrier} \quad m \tag{A-1}$$

$$Mean\_Error(t) = \max\left\{u \sin\left(2\pi \frac{t}{TL1}, FLOOR\right)\right\}, \; t < TL1/4 = \max[u, FLOOR], \quad t > TL1/4 \tag{A-2}$$

$$u = \frac{A_0}{2\pi} \; \frac{TL1}{t}, \quad TL1 = 1600 \text{ s}, A_0 = 10 \text{ m}, \; FLOOR = 0.4 \text{ m}, \sigma_{carrier} = \; 0.03 \text{ m}, \; K_{CNMP} = 3.29 \tag{A-3}$$

Residual Troposphere Error

The MS error due to residual troposphere delay error is the same as the airborne model and is used in WAAS.

$$\sigma_{tropo} = 0.12 \frac{1.001}{\sqrt{0.002001 + \sin^2(el_m)}} \quad m \tag{A-4}$$

APPENDIX B: TYPICAL SV EPHEMERIS + CLOCK COVARIANCE MATRIX

Procedure

A procedure was developed to construct a typical covariance matrix from present GPS SV data. This matrix describes the fault-free ephemeris and clock errors in HCLT coordinates. The PRN31 (Block IIRM) was selected as the representative SV. For the 4 week period of day 1 (June 29) – day 28 (July 26, 2008), PRN31 broadcast ephemeris, clock and precise ephemeris, clock data files were downloaded from the NGA website **(ftp://ftp.nga.mil/pub2/gps/apcpe/2008apc/).**

- The PRN31 position and clock were computed from the broadcast data file using the IS-GPS-200 protocol
- The PRN31 "truth" position and clock were computed from the precise file using the sp3 protocol
- The SV ephemeris and clock errors were then computed at 15 min intervals over the 4 week period
- The resulting ephemeris errors were converted from ECEF to HCLT
- The position and clock errors in HCLT from the 15 min GPS time epochs were interpolated to sidereal 15 min time epochs from day 2 to day 28
- The resulting error data were divided into 28 sidereal day ensemble sections for the computation of ensemble variance and correlation coefficient statistics for the equivalent sidereal time for each day
- The data for each of the four Sundays were discarded due to a software compatibility issue so the actual ensemble sample size is 24 rather than 28.

Equation B-1 represents the typical covariance matrix computed at some time k.

$$\mathbf{C}_0 = \begin{bmatrix} \sigma_h^2 & \rho_{hc}\sigma_h\sigma_c & \rho_{hl}\sigma_h\sigma_l & \rho_{ht}\sigma_h\sigma_t \\ \rho_{ch}\sigma_c\sigma_h & \sigma_c^2 & \rho_{cl}\sigma_c\sigma_l & \rho_{ct}\sigma_c\sigma_t \\ \rho_{lh}\sigma_l\sigma_h & \rho_{lc}\sigma_l\sigma_c & \sigma_l^2 & \rho_{lt}\sigma_l\sigma_t \\ \rho_{th}\sigma_t\sigma_h & \rho_{tc}\sigma_t\sigma_c & \rho_{tl}\sigma_t\sigma_l & \sigma_t^2 \end{bmatrix} \tag{B-1}$$

ρ: cross-correlation coefficient

The typical covariance matrix organized as in (B-1) and computed from the ensemble statistics is

$$\mathbf{C}_0 = \begin{bmatrix} 0.0608 & -0.0104 & -0.0820 & 0.2724 \\ -0.0104 & 0.2216 & -0.2415 & -0.0495 \\ -0.0820 & -0.2415 & 0.9456 & -0.4499 \\ 0.2724 & -0.0495 & -0.4499 & 1.5495 \end{bmatrix} \tag{B-2}$$

APPENDIX C: OVER BOUNDING JUSTIFICATION FOR RSS

In order to justify the use of RSS, this appendix shows that the probability (P_{ec}) of the SV ephemeris and clock component of a user's range measurement error is bounded by a normal tail probability. That is to show that

$$P_{ec} \le 2 \int_{-\infty}^{-K_I} N(x,0,1)\,dx, \ \forall K_I \tag{C-1}$$

With integrity monitoring, P_{ec} is a function of P_{fault} and $P_I\{K_I\, MMU(P_{LOIGF\_req})\}$ given by

$$P_{ec} = P_{fault} \times P_I\{K_I MMU(P_{LOIGF\_req})\} \tag{C-2}$$

$$
\begin{aligned}
&P_I\{K_I MMU(P_{LOIGF\_req})\} \\
&= \underset{b}{peak}\left[prob\left\{ |e+b| > K_I MMU(P_{LOIGF\_req}) \cap |s+b| \le T_{max} \right\} \right] \\
&= \underset{b}{peak}\left\{ \int_{K_I MMU(P_{LOIGF\_req})-b}^{\infty} \int_{-T_{max}-b}^{T_{max}-b} f(s,e)\,ds\,de + \int_{-\infty}^{-K_I MMU(P_{LOIGF\_req})-b} \int_{-T_{max}-b}^{T_{max}-b} f(s,e)\,ds\,de \right\}
\end{aligned}
\qquad \text{(C-3)}
$$

See (9 - 11) for notation definition

Recall from (6), $P_{LOIGF\_req} = 10^{-8} / P_{fault}$. Therefore, $MMU(P_{LOIGF\_req})$ can be considered a function of P_{fault}. Since MMU_{PL} in (16) is the selected MMU, $MMU(P_{LOIGF}) = MMU_{PL}$. K_{md} is selected to correspond to any desired value of P_{fault}, P_{LOIGF_req}. Table C-1 shows values of K_{md} and resulting $MMU(P_{LOIGF\_req})$ that would be used for values of $P_{fault} = 1, 10^{-2}, 10^{-3}, 10^{-4}$.

Figure C-1 is based on the same inputs that were used to construct Figure 2. To illustrate the range of over bounding as a function of P_{fault}, Figure C-1 contains plots of P_{ec} that show where the over bounding inequality (C-1) is achieved. Over bounding is achieved whenever P_{ec} is below the Gaussian tail probability in the left figure. The right figure, a plot of the ratio of Gaussian tail probability / P_{ec} versus Gaussian tail probability, indicates over bounding when the ratio ≥ 1. From the figure it is seen that over bounding occurs only when $P_{fault} \le 10^{-3}$ / h. (Actually maximum allowable P_{fault} is a value somewhere between 10^{-2} and 10^{-3}.)

Table C-1. K_{md} and $MMU(P_{LOIGF\_req})$ Corresponding to P_{fault}

P_{fault}	P_{LOIGF_req}	K_{md} corresponding to P_{LOIGF_req} (1-sided)	$MMU(P_{LOIGF\_req})$
1	10^{-8}	5.62	1.04 m
10^{-2}	10^{-6}	4.76	0.96
10^{-3}	10^{-5}	4.27	0.91
10^{-4}	10^{-4}	3.72	0.86

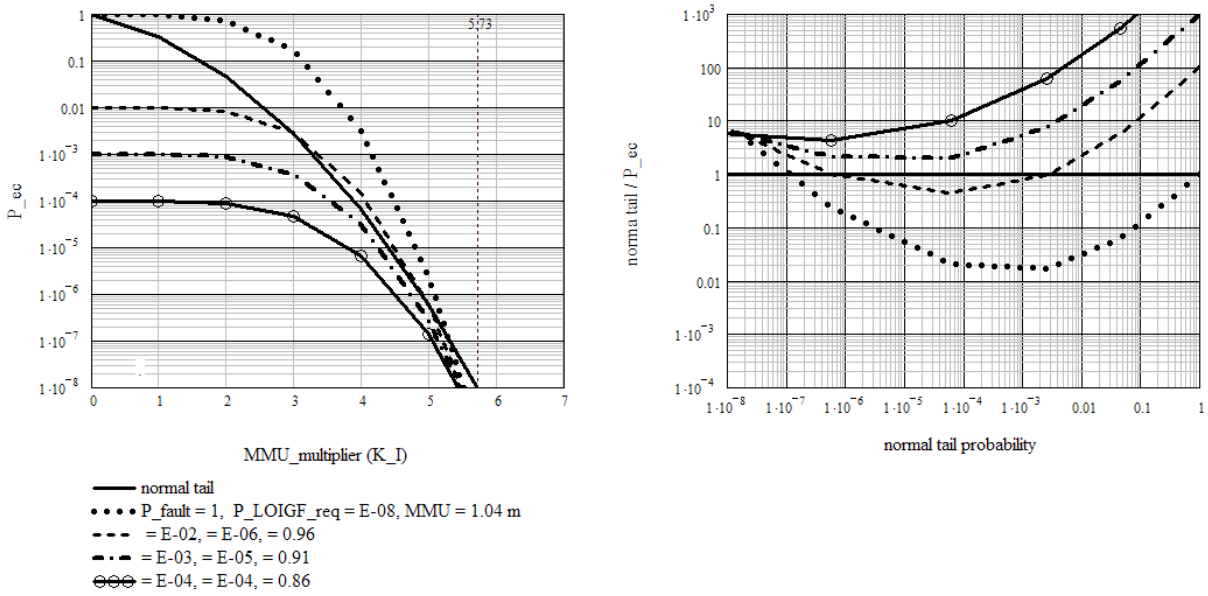

Figure C-1. Illustrating Normal Distribution Over Bound for Various Values of P_{LOIGF_req}